



CHORUS

This is the accepted manuscript made available via CHORUS. The article has been published as:

Direct Heating of a Laser-Imploded Core by Ultraintense Laser-Driven Ions

Y. Kitagawa *et al.*

Phys. Rev. Lett. **114**, 195002 — Published 12 May 2015

DOI: [10.1103/PhysRevLett.114.195002](https://doi.org/10.1103/PhysRevLett.114.195002)

Direct Heating of a Laser-Imploded Core by Ultra-Intense Laser-Driven Ions

Y. Kitagawa,* Y. Mori, O. Komeda, K. Ishii, R. Hanayama, K. Fujita, and S. Okihara

*The Graduate School for the Creation of New Photonics Industries,
Kurematsucho, 1955-1 Nishi-ku, Hamamatsu 431-1202 Japan*

T. Sekine, N. Satoh, T. Kurita, M. Takagi, T. Watari, T. Kawashima, and H. Kan

*Hamamatsu Photonics, K. K. Kurematsucho,
1820 Nishi-ku, Hamamatsu 431-1202 Japan*

Y. Nishimura

*Toyota Technical Development Corp., 1-21 Imae,
Hanamoto-cho, Toyota, Aichi, 470-0334 Japan*

A. Sunahara

Institute for Laser Technology, 1-8-4 Utsubo-honmachi, Nishi-ku, Osaka, 550-0004 Japan

Y. Sentoku

*Department of Physics, University of Nevada,
Reno 1664 N VIRGINIA ST Reno, NV 89557*

N. Nakamura, T. Kondo, and M. Fujine

*Advanced Material Engineering Div., TOYOTA Motor Corporation,
1200, Mishuku, Susono, Shizuoka, 410-1193 Japan*

H. Azuma, T. Motohiro, T. Hioki, and M. Kakeno

*TOYOTA Central Research and Development Laboratories,
Inc., 41-1Yokomichi, Nagakute-cho, Aichi, Japan*

E. Miura

*National Institute of Advanced Industrial Science and Technology,
1-1-1 Umezono, Tsukuba, Ibaraki 305-8568 Japan*

Y. Arikawa, T. Nagai, and Y. Abe

*Institute of laser Engineering, Osaka University,
2-6 Yamadaoka, Suita, Osaka 565 Japan*

S. Ozaki

*National Institute for Fusion Science,
322-6 Oroshi Toki, Gifu 509-5292 Japan*

A. Noda

*Advanced Research Center for Beam Science,
Institute for Chemical Research, Kyoto University,
Gokasho, Uji, Kyoto 611-0011 Japan*

(Dated: Received: March 4, 2014, Revised:)

A novel direct core heating fusion process is introduced, in which a preimploded core is predominantly heated by energetic ions driven by LFEX, an extremely energetic ultra-short pulse laser. Consequently, we have observed the $D(d, n)^3He$ -reacted neutrons (DD beam-fusion neutrons) with the yield of 5×10^8 n/4 π sr. Examination of the beam-fusion neutrons verified that the ions directly collide with the core plasma. While the hot electrons heat the whole core volume, the energetic ions deposit their energies locally in core, forming hot spots for fuel ignition. As evidenced in the spectrum, the process simultaneously excited thermal neutrons with the yield of 6×10^7 n/4 π sr, raising the local core temperature from 0.8 keV to 1.8 keV. One dimensional hydrocode, STAR 1D, explains the shell implosion dynamics including the beam fusion and thermal fusion initiated by fast deuterons and carbon ions. Two-dimensional collisional particle-in-cell code predicts the core heating due to resistive processes driven by hot electrons, and also generation of fast ions, which could be additional heating source when they reach the core. **Since the core density is limited to 2 g/cm³ in the current experiment, neither hot electrons nor fast ions can efficiently deposit their energy and the neutron yield remains low. In future work, we will achieve the higher core density (>10 g/cm³), then hot electrons could contribute more to the core heating via drag heating. Together with hot electrons, the ion contribution to fast ignition is indispensable for realizing high-gain fusion. By**

virtue of its core heating and ignition, the proposed scheme can potentially achieve high gain fusion.

PACS numbers: 52.57.-z, 52.57.Fg, 79.20.Eb, 42.55.X, 28.52.Cx

The nuclear fusion power is one of the ultimate and safe energy sources for the mankind. High-density compression and core heating are essential processes in inertial confinement fusion. In the fast ignition scheme of Tabak et al. [1], a preimploded deuterium-tritium capsule is irradiated with a laser pulse for a few tens of picoseconds, generating energetic electrons. These electrons are transported through the plasmas to the core, where they are expected to form a hot spot. The fast heating and ignition will powerfully help the inertial confinement fusion to produce energy, if it succeeds in triggering the core ignition with high gain.

In previous fast heating studies, a petawatt laser[2] enhanced the neutron yields to the order of 10^6 n/4 π sr [3–5]. However, 2-D simulations and experiments suggest that the hot electrons diverge, thereby heating the whole core area rather than a local region [6–11]. Energetic ion contributions cannot be ignored in neutron enhancement estimates.

We propose a new scheme that directly heats imploded cores by energetic ions driven by an ultra intense laser LFEX. The laser drives both hot electrons and energetic ions around the critical density. Fractions of these

driven particles are transported through the overdense plasma to the core. Hot electrons will heat the whole core, while energetic ions will deposit their large amount close to the core periphery, locally heating it to the ${}^4\text{He}$ (α particle) burning temperature. An α burning wave then spreads from the hot spot over the core. Observation of beam-fusion neutrons verified that the energetic ions predominantly heat the imploded core and likely form ignition spots.

Here, as shown in Fig.1(a), a spherical deuterated polystyrene (C_8D_8 or CD) shell was polarly imploded by two counter beams of a GEKKO XII (GXII) green laser. To directly heat the core, we focused LFEX onto the naked core from the side, vertical to the GXII axis. By illuminating LFEX to the core as close as possible, we found that both the hot electrons and energetic ions play important roles in core heating. In fact, DD beam-fusion neutrons with the yield of 5×10^8 n/4 π sr are observed.

Observation both of the beam- and thermal-fusion neutron peaks indicate that the laser-driven ions (deuteron and carbon⁺⁶) not only drive the beam-fusion reaction, but also contribute to the core heating. Compar-

ing the spectral broadening of the thermal neutron peak with 1D simulation, we estimated that the peripheral core temperature rose twofold (from 0.8 keV to 1.8 keV). The incremented core temperature was supported by X-ray emissions.

10^{10} n/sr neutron yield was thus far achieved by short pulses of a 200 TW laser in a double target (a CD₂ foil and a vacuum-separated Be converter) scheme [12]. The ponderomotive force of the short pulse laser drives hot electrons at the critical density, which drag ions away from the rear side of the thin foil target [13–15]. The energy gain G of the ions is given by $G = (1 + a_0^2/2)^{1/2} m_e c^2$, where $a_0 = eE_L/m_e\omega c$ for the electron mass m_e and the laser field E_L of the frequency ω [14]. In Roth's scheme, the first target is for ion acceleration (pitcher) by irradiating an intense laser pulse and the second one is for the fusion reactions (catcher, Be), so that the scheme is basically the beam fusion, does not heat the target itself, namely, no thermal fusion. The neutrons here are produced in a combination of beam fusion and thermal fusion in a compressed deuterated core plasma. **There have been some theoretical fast ignition works with proton by Roth et al.[16] and proton and other ion beams by M. Temporal et al.[17] and J. C. Fernandez et al.[18].**

Since the target is imploded by two counter beams of the GXII, an undressed core

area is created vertical to the beam axis. The diameter and thickness of the target are $7\ \mu\text{m}$ and $500\ \mu\text{m}$, respectively [Fig. 1(b)]. The target has two $250\text{-}\mu\text{m}$ diameter holes, one to guide the LFEX beam into the target and the other to ventilate the preplasmas generated by the GXII. The latter hole is not for heating, but enables direct detection of X-rays and charged particles emitted from the heated core. Figure 1(c) shows the configuration of the target, lasers, and detectors. Each of the two counter beams from the GXII carries 254 ± 14 J in a 1.3-ns-wide Gaussian pulse at a wavelength of $0.527\ \mu\text{m}$. An aspheric lens (F-number 3) focuses each beam onto position $d = -400\ \mu\text{m}$ from the target center ($d/R = -1.6$). The intensity of the beam on the target is 3.1×10^{14} W/cm².

At the maximum compression time, we focused LFEX onto this undressed area. The cross section of the LFEX beam is $80\ \text{cm} \times 40\ \text{cm}$. An off-axial parabolic mirror with a focal length of 4 m (F-number 10) focuses 50% of the 613 J at a wavelength of $1.053\ \mu\text{m}$ onto a $60\text{-}\mu\text{m}$ -diameter spot, producing an intensity of 1×10^{19} W/cm² in vacuum. The LFEX and GXII beams are electronically synchronized (jitter < 100 ps).

Figure 1(d), an image from the X-ray streak camera (XSC), shows the implosion flow driven by the two GXII counter beams and the core emission without LFEX illumi-

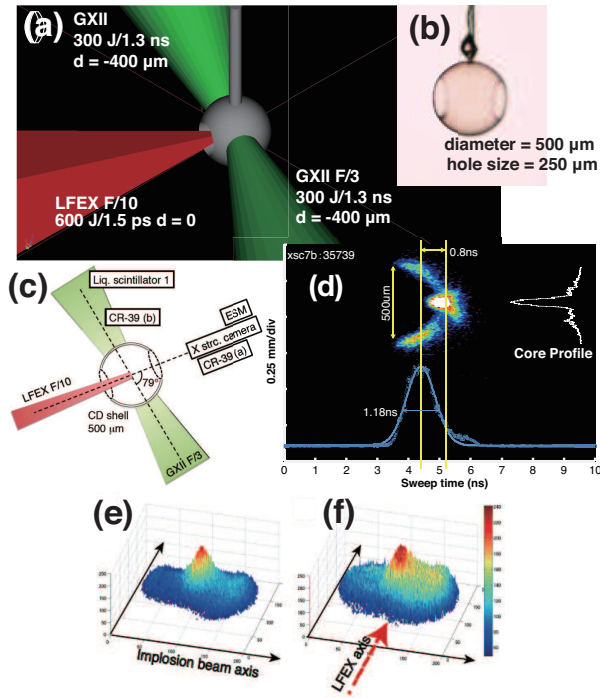


FIG. 1. (a) CD shell counter-imploded by two GXII beams and 79°-side heated by LFEX. (b) Shell with two holes for LFEX introduction and for preplasma ventilation. (c) The target, lasers, and detectors. (d) X-ray streak image of the shell flow: two GXII beams arrive from the upper and lower sides. The rightmost trace is the core profile without LFEX illumination. Horizontal axis: 1 ns/div, vertical axis: 250 μm/div (Hamamatsu Photonics C4575-03). (e) Time-integrated X-ray pinhole image without and (f) with LFEX (shot #35732).

nation. The bottom plot represents the imploding shell emission trajectory, which follows the GXII pulse shape. One dimensional hydrocode, STAR 1D, predicts the maximum

compression of the core 0.9 ns after the implosion beam peak, while XSC shows in Fig. 1(d) that the emission peak is 0.8 ns, probably due to the hot electron or shock preheating.

The core diameter is $55 \pm 1 \mu\text{m}$ in full width at half maximum (FWHM). Assuming that the imploding beams converge two $(200 \times 200 \times 7) \mu\text{m}^3$ shell volumes into a 55-μm-wide and 230-μm-long ellipsoidal core, the material is compressed to at least twice its solid density (2 g/cm^3). Although STAR 1D predicts the $5 \sim 10 \text{ g/cm}^3$ compression of the core, the narrow width of the beam cone angle (19°) realizes only twice the solid density under 2D expansion. STAR 1D estimated also that the core radius and temperature at the maximum compression are $35 \mu\text{m}$ and $\sim 0.8 \text{ keV}$, respectively.

We examined the effect of the two holes on the counter beam implosion. The XSC showed no difference between the flow diagrams of the shells with and without holes. The intensities of the core emission were the same.

Figure 1(e) displays the time-integrated X-ray pinhole images in 2-3 keV energy range without LFEX. The emission size is $360 \mu\text{m}$ FWHM along the GXII beam, while it is $230 \mu\text{m}$ along the LFEX axis: therefore, the LFEX absorption point is 0.6 times closer to the core than expected in a uniform implosion. As indicated by an arrow in Fig. 1(f),

we illuminated LFEX at the time of peak core emission. The core shape was not so changed except that the total X-ray intensity increased by 8 % in 2-3 keV range.

The neutron time-of-flight (TOF) signals were detected by two gated oxygen-enriched liquid scintillators [22]. Liquid scintillator LS1 was set 13.35 m from the target at 69.13° (right-forward) to the LFEX incidence (in the horizontal direction); liquid scintillator LS2 was set 2.5 m from the target perpendicular to the LFEX axis. To prevent γ noises, we electronically gated the photomultiplier dynode prior to the arrival of the neutron signals.

Before illuminating LFEX, we confirmed that the neutrons were generated from the core and not from the shell. The yield without LFEX was $10^5 \sim 10^6$ n/4 π sr/shot: LS2 detected 7×10^5 (#35739). The TOF signals from LS1 without LFEX are shown in Fig. 2(a). Illumination by both GXII and LFEX lasers shows a large DD neutron yield (the TOF signal and its energy spectrum are shown in Figs. 2(b) and (c), respectively). The solid angle and sensitivity of LS1 are 1.4×10^{-4} sr and 1 count/5.6 neutrons, respectively.

The neutron signals in Fig. 2(c) were fitted by a two-peak Gaussian curve: $dN/dE = 1 \times 10^7 + 9.8 \times 10^7 \exp -[(\sqrt{E} - \sqrt{3.3})^2/0.01] + 4.9 \times 10^7 \exp -[(\sqrt{E} - \sqrt{2.5})^2/0.0025]$, where

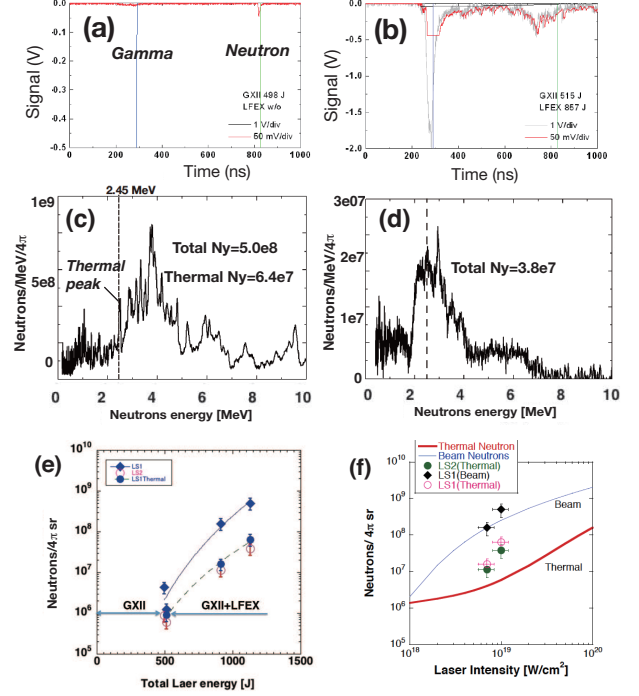


FIG. 2. (a) Neutron and γ TOF signals from LS1 : Shot #35739 of 498-J GXII without LFEX, and (b) Shot #35732 of 515-J GXII + 613-J LFEX. (c) Neutron energy spectrum, converted from (b). Small peak at 2.45 MeV is a thermal peak with a yield of 6.4×10^7 n/4 π sr. Large peak is a beam-fusion peak with 5×10^8 n/4 π sr. (d) Spectrum from LS2. (e) Neutrons from LS1 (thermal: solid circles; beam: diamonds) and LS2 (thermal+beam: open circles) versus GXII+LFEX laser energy E . The instrumental and calibration error is 32%. The dashed line is proportional to E^5 . (f) STAR 1D: beam- and thermal-fusion yields versus LFEX intensity on the target. Solid lines are the beam- and dotted are thermal-fusion, respectively. Diamonds and circles are the experiments in (e).

the energy unit is MeV. The second term on the right-hand side describes the main peak in Fig.2(c), which is up-shifted from 2.45 MeV to 3.3 MeV. Although LS1 was angled -69.13° (right-forward) from the LFEX axis, we infer that the peak at 3.3 MeV arises from beam fusion (width ΔE_B is $0.01 \text{ MeV} \times \ln 2 = 6.9 \text{ keV}$ at HWHM). The third term describes the peak at 2.5 MeV (width ΔE_T is $0.0025 \text{ MeV} \times \ln 2 = 1.7 \text{ keV}$ at HWHM), and is inferred as the core temperature. Integrating the curve from 2 to 6 MeV and normalizing by $4\pi \text{ sr}$, we obtain the yield of $(5.1 \pm 1.6) \times 10^8 \text{ n}/4\pi \text{ sr}$. The peak at 2.5 MeV corresponds to $6.4 \times 10^7 \text{ n}/4\pi \text{ sr}$ (13% of the total yield), indicating that thermal neutrons have been enhanced 100-fold from $5 \times 10^5 \text{ n}/4\pi \text{ sr}$ and that the core temperature has roughly doubled from 0.8 keV to 1.8 keV. From the Planck relation, the X-ray pinhole emission of 2-5 keV infers the core temperature to be 0.8–2 keV[23].

LS2 signals in Fig.2(d) feature a single broad peak around 2.45 MeV. The total yield normalized by $4\pi \text{ sr}$ is $3.8 \times 10^7 \text{ n}/4\pi \text{ sr}$, of the same order as the 2.45 MeV peak yield in the LS1 signal (Fig. 2(c)).

In Fig.2(e) the 4π angle neutron yields from LS1 and LS2 are plotted as functions of the total laser energy E (LFEX+GXII). No LFEX is illuminated up to 500 J. The solid circles indicate the neutrons yielded by ther-

mal fusion at around 2.45 MeV. The dashed line in Fig.2(e) is proportional to E^5 and represents the best fit to the experimental data. Assuming that the core temperature T_c is proportional to E and the thermal yield is proportional to T_c^5 , an increase from 500 J to 1.1 kJ corresponds to a T_c increase from 0.8 to 1.8 keV, raising the yield from 5×10^5 to $2.5 \times 10^7 \text{ n}/4\pi \text{ sr}$.

The neutron yields were confirmed by STAR1D assuming 50% absorption by the hot electrons with the 4-MeV-slope temperature and 1.3% conversion to carbon⁺⁶ and deuteron⁺¹ at a laser intensity of $1 \times 10^{19} \text{ W}/\text{cm}^2$. The temperatures of the bulk electrons and of the ions are 1.8 keV close to the surface and 1.0 keV far from the surface, respectively. Figure 2(f) plots the STAR1D lines as functions of the LFEX intensity. Deuterons and carbons are related to beam fusion and thermal fusion lines, respectively. The diamonds and solid circles are the experimental points in Fig.2(e).

We positioned two CR-39 ion-track detectors (a) at 20.9° and (b) 109° relative to the LFEX incidence. The signals detected at (a) have traveled straight throughout the core and are shown in Fig.3(a); the side signals detected at (b) are shown in Fig.3(b). Both detectors are positioned 10 cm from the target. The counting areas of both detectors is 0.0227 mm^2 , implying a detection solid angle

of 2.3×10^{-6} sr. Before the LFEX arrives at the target, the GXII laser illumination ablates and removes the surface hydrocontamination layers. Therefore, the LFEX heats pure CD plasma, producing only hot electrons, energetic carbons and deuterons.

Deuterons of Fig. 3(a) are rarely observed below 1 MeV, comparing with those of (b). The deuterons generated at the cutoff density must include energies from below 1 MeV to above a few tens MeV[25]. As suggested in Fig. 4(d), these deuterons must be emitted over broad solid angles. Therefore, those coming from the core, Fig. 3(a), must be stopped. Figure 3(b) seems to show that the side scattered ones are not stopped. Their non-exponential decay must be the result of capturing additional deuterons, pulled by runaway hot electrons, which explains the large count difference between the signals (a) and (b) (71 counts of Fig. 3(a) versus 231 counts of Fig. 3(b)).

From the 2D rad-hydro calculations, the peak density and size of the core plasma were determined as 2 g/cm^3 and $230 \mu\text{m}$, respectively. Using these values, we calculated the deuteron stopping range in fully-ionized CD plasmas at various initial energies and are plotted in Fig. 3(c). Deuterons of 0.9 MeV or less are stopped by the $230 \mu\text{m}$ core, consistent with the results of Fig. 3(a).

According to the STAR 1D (see Fig. 3(d)),

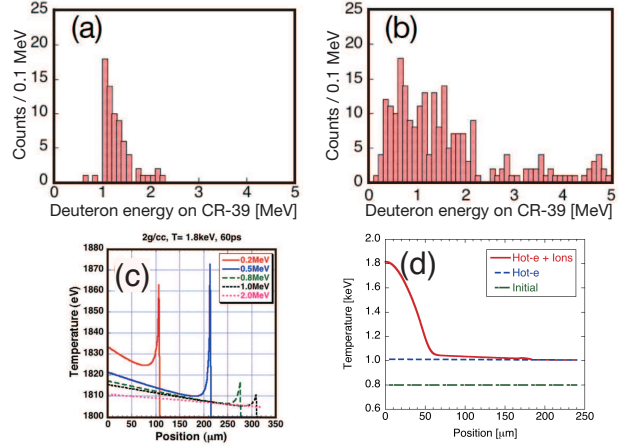


FIG. 3. (a) Ion spectrum of shot #35737 from CR-39 track detector (a). 71 counts are detected. (b) Spectrum from the detector (b). 231 counts are detected. Both detectors comprise a $20\text{-}\mu\text{m}$ -thick aluminum filter and three stacks of $100\text{-}\mu\text{m}$ -thick CR-39 films. (c) STAR 1D-simulated temperature profile of the CD plasma, heated by the slowdown of the injected fast deuterons. The initial energy of the deuterons is 0.2, 0.5, 0.8, 1.0 and 2.0 MeV. (d) STAR 1D simulations: 50% absorption of hot electrons heats the core to 1 keV. Fast carbons heat the core surface from 1 keV to 1.8 keV. Core edge and center are 0 and $240 \mu\text{m}$, respectively.

hot electrons heat the entire core from 800 eV to 1 keV, whereas carbon⁺⁶ predominantly heats the region $20 \mu\text{m}$ from the core surface from 1 keV to 1.8 keV. The thermal- and beam-fusion yields are 2.3×10^7 and $4.1 \times 10^8 \text{ n}/4\pi \text{ sr}$, respectively, consistent with observations. Although the beam fusion neutrons were not uniformly distributed over all

solid angles, we estimated the 4π sr yield for comparison with the 1D simulations.

An electron spectrometer placed on the LFEX axis detected hot electrons throughout the core with a 5.5-MeV-slope temperature.

Particle-in-cell (PIC) simulations predict that hot electrons spread over $\sim 60^\circ$. The present path to the core area, however, is so short ($100\ \mu\text{m}$), that more than a third (33%) of the hot electrons strike the core plasma and deposit their energy [5].

Once the initial density and temperature at the maximum compression are determined by STAR 1D (see Figs. 4(a) and (b)), the energetic particle generation and heating by LFEX is verified in a 2D collisional PIC simulation (PICLS)[26]. PICLS evaluated the mechanism by which the bulk electrons are heated and the heat is transported to the core, as shown in Fig. 4(a). The bulk electron temperature exceeds 1 keV in the core region at 2 ps. The fast-electron current ohmic-heats the deuterons to a few hundred electron volts at the core periphery ($\sim 1\ \text{g}/\text{cm}^3$ at $x = 160\ \mu\text{m}$): see in Fig. 4(b). The collisionless shock accompanying the deuterons with MeV energies arrives at the core later than the 2 ps simulation time. As shown in Fig. 4(b), the shock front appears at around $x = 100\ \mu\text{m}$ at 2 ps. High energy deuterons will reach the core region a few picoseconds later and deposit additional energy. Fig-

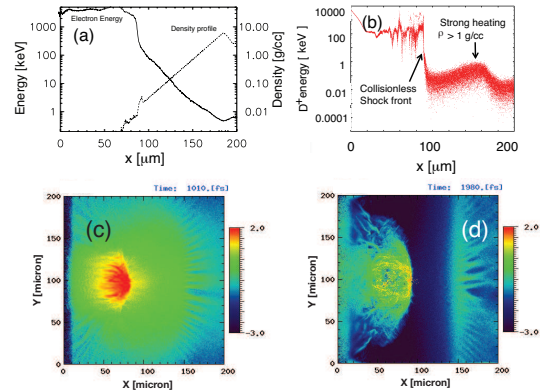


FIG. 4. (a) PICLS coupled to STAR 1D: bulk electron temperature profile at 2 ps. Core is heated to ~ 1 keV. (b) Deuteron energy profile, heated to a few 100 eV at $x \sim 160\ \mu\text{m}$. (c) 2D electron energy density at 1 ps and (d) deuteron energy density at 2 ps. X-axis is the laser propagation direction. $x = 0\ \mu\text{m}$: vacuum; $x = 100$: cut-off; $x = 200$: core center. Y-axis is the vertical direction. CD plasma peak density is $\sim 6\ \text{g}/\text{cm}^3$ and core density $\sim 2\ \text{g}/\text{cm}^3$. Laser is emitted at $10^{19}\ \text{W}/\text{cm}^2$, 1.5 ps pulse length, $60\ \mu\text{m}$ focal spot. Assuming the absorbing boundary condition, we detected 675 million particles in 5000×5000 grids and performed up to 2 ps of simulation using 200 cores of AMD processors.

ures 4(c) and (d) show the 2D profiles of the electron energy density at 1 ps and the deuteron energy density at 2 ps, respectively. The resistive processes driven by hot electrons and generation of fast ions, could be additional heating source when they reach the core. Coupling PICLS to two-dimensional

STAR code will be done in future.

In conclusion, the preimploded core of the CD shell target was heated by direct illumination of LFEX, yielding 5×10^8 DD neutrons by deuteron-beam fusion. This result verifies that the core is locally heated by ions. Thermonuclear neutrons are driven by energetic ions such as carbon⁺⁶. STAR 1D results reasonably agreed with the experiments. LFEX increased the core temperature from 0.8 keV to 1.8 keV locally on its periphery. PICLS coupled to STAR 1D could evaluate the bulk heating and heat transport mechanism by the LFEX driven electrons and ions. Our implemented polar implosion scheme achieves the advantage of predominant ion heating by placing the ignition laser closer to the core than in spherical implosion schemes.

While the hot electrons heat the whole core volume, the energetic ions locally deposit heat to form ignition spots. However, since the core density is limited to 2 g/cm^3 in the current experiment, neither hot electrons nor fast ions can efficiently deposit their energy and the neutron yield remains low. In future work, we will achieve the higher core density ($>10 \text{ g/cm}^3$), then hot electrons could contribute more to the core heating via drag heating. Also we will apply a higher power laser (e.g. 10^{20} W/cm^2) to increase the energy carried by fast ions, and then the ion contribution will be much more significant.

Together with the hot electrons, the ion contribution to fast ignition is indispensable for realizing high-gain fusion. The polar implosion can be feasibly adopted in demonstration machines and commercial power plants, provided that the additional fast core heating compensates the nonuniform implosion caused by the polar illumination.

This study was conducted under the collaborative program of the Institute of Laser Engineering (ILE), Osaka University. We would like to thank the LFEX and GXII operation, measurement, and target fabrication teams at the ILE. We also thank Y. Sakawa of ILE for their contributions to this study. Y.S is supported by NNSA/US DOE under Contracts DE-FC02-04ER54789 and DE-SC0008827.

* kitagawa@gpi.ac.jp

- [1] M. Tabak *et al.*, Phys. Plasmas **1**,1626 (1994).
- [2] Y. Kitagawa *et al.*, IEEE J. Quantum Electron. **71**, 281-293 (2005).
- [3] R. Kodama *et al.*, Nature(London) **412**, 798-802 (2001).
- [4] R. Kodama *et al.*, Nature(London) **418**, 933-934 (2002).
- [5] Y. Kitagawa *et al.*, Phys. Rev. E **71**, 016403-1-5 (2005).

- [6] S. Atzeni, J. Meyer-ter-Vehn, “*The Physics for Inertial Fusion, Beam Plasma Interaction, Hydrodynamics, Hot Dense Matter*” Oxford Science Publications, 2004.
- [7] Y. Sentoku *et al.*, Phys. Plasmas **11**, 3083 (2004).
- [8] R. Jung *et al.*, Phys. Rev. Lett. **94**, 195001-1-4 (2005).
- [9] A. L. Lei *et al.*, Phys. Rev. Lett. **96**, 255006 (2006).
- [10] N. Naumova *et al.*, Phys. Rev. Lett. **102**, 025002 (2009).
- [11] Y. Kitagawa *et al.*, Phys. Rev. Lett. **108**, 155001 (2012).
- [12] M. Roth *et al.*, Phys. Rev. Lett. **110**, 044802 (2013).
- [13] Y. Murakami *et al.*, Phys. Plasmas **8**, 4138-4143(2001).
- [14] T. Sentoku *et al.*, Appl. Phys. **74**, 207 (2002).
- [15] B. J. Hegelich *et al.*, Nature (London) **439**, 441-444 (2006).
- [16] M. Roth *et al.*, Phys. Rev. Lett. **86**, 436-439 (2001).
- [17] M. Temporal, J. J. Honrubia and S. Atzeni, Phys. Plasmas **9**, 3098-3107 (2002).
- [18] J. C. Fernandez *et al.*, Nuclear Fusion **54**, 054006 (2014).
- [19] P. Norreys *et al.* Plasma Phys. Control. Fusion **40**, 175-182 (1998).
- [20] W. Theobald *et al.*, Phys. Plasmas **18**, 056305 (2011).
- [21] A. Sunahara *et al.*, Plasma Fusion Res. **3**, 043-1-5 (2008).
- [22] Y. Arikawa *et al.*, Rev. Sci. Instrum. **83**, 10D909 (2012).
- [23] Ya. B. Zel’dovich and Yu. P. Raizer, *Physics of Shock Waves and High-temperature Hydrodynamic Phenomena*, Vol.I, p.116, Academic Press, New York, 1967.
- [24] Y. Sentoku *et al.* Fusion Sci. Technol. **49**, 278 (2006).
- [25] S. C. Wilks, W. L. Kruer, IEEE J. Quantum Electronics, **33**, 1964-1968 (1997).
- [26] Y. Sentoku, A. J. Kemp, J. Comp. Phys. **227**, 6846 (2008).